Research paper

Rational design of Si/TiO$_2$ heterojunction photocatalysts: Transfer matrix method

Xiaolong Yao[a], Lei Chen[a], Mengyin Liu[a], Deqiang Feng[a], Changhong Wang[a], Feng Lu[a], Weihua Wang[a], Xuewei Wang[b], Yahui Cheng[a], Hui Liu[a], Haijun Chen[a,*], Weichao Wang[a,c,*]

[a] Department of Electronics and Tianjin Key Laboratory of Photo-Electronic Thin Film Device and Technology, Nankai University, Tianjin, 300071, China
[b] School of Materials Science and Engineering, Tianjin University of Technology, Tianjin 300384, China
[c] Department of Materials Science & Engineering, the University of Texas at Dallas, Richardson, TX 75252, USA

ARTICLE INFO

ABSTRACT

The charge transfer in semiconductor heterojunction photocatalyst is one of the key factors determining its catalytic efficiency and durability in an aqueous environment. The widely used interface model with the simplified rectangular potential barrier fails to precisely predict the carrier transfer process since the band bending and its variation caused by solar energy are both not considered. Here, utilizing transfer matrix method, we take the Si/TiO$_2$ heterojunction as a prototype to shed light on the rational design of the semiconductor heterojunction photocatalyst in terms of its intrinsic characteristics, such as TiO$_2$ thickness and the dopant concentration. We find that the minimum incident energy (MIE) for electrons (holes) tunneling through the Si/TiO$_2$ heterojunction decreases (increases) as the thickness of TiO$_2$ layer increases. Within a moderate condition (TiO$_2$ thickness of 3 nm and dopant concentration of 1×10^{18} cm^{-3} (5×10^{19} cm^{-3}) in Si (TiO$_2$)), both electrons and holes can transfer through the heterojunction barrier with relatively small incident energy. Furthermore, the photovoltage under illumination is beneficial for reducing MIE for electrons while increasing that for holes. Therefore, our transfer matrix scheme provides insights into rational design of the high efficient photocatalyst.

1. Introduction

The development of semiconductor photocatalysts for water splitting to produce hydrogen using solar energy has undergone considerable research over past decades [1–9]. Constructing semiconductor heterojunctions has been shown to be an effective scheme for improving photocatalytic activity through high efficient photogenerated charge separation and transfer [9–11]. However, a fundamental understanding of the charge transfer in semiconductor heterojunction photocatalysts remains unclear due to the complexity of band structure at heterojunction interface. To date, the extensively adopted interface models for designing and optimizing semiconductor heterojunction photocatalysts are based on the simplified rectangular potential energy barrier, including the Z-scheme [12–16] and the type-II (staggered) heterostructures [17–20]. The fatal weakness of these interface models is the ignorance or only schematically describing band bending at the semiconductor interface that could decisively affect the interfacial charge transfer process [11,21]. Another factor strongly influencing the interfacial potential barrier is the photovoltage emerging under illumination, which is even harder to be considered in above discussed interface models.

Because of these severe deficiencies, the present interface models cannot accurately predict the photocatalytic activity thus direct the design of semiconductor heterojunction photocatalysts. Here, we utilize the transfer matrix method to quantitatively investigate the dependence of band bending and photovoltage on the charge transfer in a prototype Si/TiO$_2$ heterojunction photocatalyst. This system is widely explored in experiments which in turn validates our predications.

Si has been demonstrated to be efficient for solar hydrogen production [22–24] because of its suitable band gap (1.12 eV) for absorbing sunlight. However, it is challenging to apply Si for photocatalyst directly since it easily corrodes in an aqueous environment [25]. On the other hand, TiO$_2$ is a good passivation material due to its high resistance to photocorrosion, but its conversion efficiency of solar energy to hydrogen is still low because of its large bandgap (E$_g$ = 3.0 ~ 3.2 eV) [6,26–31]. These drawbacks can be overcome by constructing the Si/TiO$_2$ heterojunction photocatalytic system, which provides a higher stability and a larger open circuit voltage [10,11,31–36].

The band bending at semiconductor heterojunction interface is

determined by the semiconductor material's intrinsic characteristics, for example, the thickness of TiO_2 protective layer and the dopant concentrations of heterojunction components. Therefore, these intrinsic characteristics of semiconductor heterojunction are fundamental factors for the design and optimization of semiconductor heterojunction photocatalysts. When the thickness of TiO_2 protective layer is small enough that the majority carriers (electrons) in TiO_2 layer are completely depleted, the energy band bending in the Si/TiO_2 heterojunction in contact with an electrolyte [37] is quite different from the situation in n-Si/n-TiO_2 heterojunction reported previously where a field-free region may exist inside the TiO_2 layer since the deposition thickness is relatively large [11,37]. On the other hand, in previous work, the complex tunneling potential barriers for charge carriers in heterojunction are simplified as rectangular potential barriers formed by the band edges of the heterojunction components neglecting the band bending in order to characterize the charge transfer process more conveniently [38,39]. Thus, the above-mentioned simplification of tunneling potential cannot accurately describe the realistic charge transfer behavior in semiconductor heterojunction.

In this paper, we apply the transfer matrix method to calculate the transmission coefficients [40–42] of charge carriers tunneling through the Si/TiO_2 heterojunction. We firstly consider the simplified rectangular potential barriers at heterojunction interface. Next, the modification of band structure including band bending and photovoltage is taken into account for revealing the dependence of charge carriers' transmission coefficients on the TiO_2 layer thicknesses and dopant concentrations in heterojunction components. It is found that the MIE for charge carriers tunneling through the Si/TiO_2 heretostructures is closely related to the TiO_2 layer thickness and the dopant concentration. The moderate condition of TiO_2 thickness (3 nm) and the dopant concentration (1×10^{18} cm^{-3} for Si and 5×10^{19} cm^{-3} for TiO_2) is beneficial for electrons and holes tunneling through the heterojunction with relatively low incident energy. Our work reveals that the intrinsic characteristics of Si/TiO_2 heterojunction photocatalysts have decisive influence on their charge transfer and essentially influence the photoactivity without considering the variation of the morphology. These rules can be generalized to design other semiconductor heterojunction photocatalysts.

2. Transfer matrix method

The transfer matrix method can be utilized to study the transport property of charge carriers in heterojunction photocatalysts by quantitatively calculating the transmission coefficients for carriers tunneling through a one-dimensional potential energy barrier with arbitrary shape [40]. In this method, the total potential energy is divided into a series of rectangular potential energy as shown in Fig. 1. This method will be accurate if the total number of rectangular potential energy N is
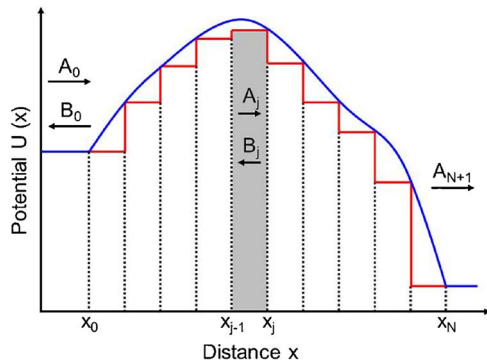

Fig. 1. The one-dimensional potential energy profile with arbitrary shape (blue line) and its approximate potential energy profile (red line) composed by a series of rectangular potential energies (gray rectangle). (For interpretation of the references to colour in this figure legend, the reader is referred to the web version of this article.)

large enough that the width of each rectangular potential energy is much smaller than the de Broglie wavelength of charge carrier [43].

Consider a particle that approaches an arbitrarily shaped one-dimensional potential barrier from the left with an incident energy E and a mass m^* (Fig. 1). In quantum mechanics, the motion of the particle is described by a complex wave function ψ that is a solution to the time-independent Schrödinger equation:

$$-\frac{\hbar^2}{2m^*}\frac{d^2}{dx^2}\psi(x) + U(x)\psi(x) = E\psi(x) \tag{1}$$

This wave will be partially transmitted through the barrier and partially reflected when it propagates to the rectangular potential barrier U_j, so the wave functions in intervals (x_{j-1}, x_j) and (x_j, x_{j+1}) are:

$$\psi_j(x) = A_j e^{ik_jx} + B_j e^{-ik_jx} \tag{2}$$

$$\psi_{j+1}(x) = A_{j+1}e^{ik_{j+1}x} + B_{j+1}e^{-ik_{j+1}x} \tag{3}$$

where A_j (B_j) is the amplitude of the transmission (reflection) wave and $k_j = \frac{1}{\hbar}(2m^*(E - U_j))^{\frac{1}{2}}$ is the wave vector within the reduced Planck's constant $\hbar$.

Due to continuity of $\psi_j(x)$ and $\frac{1}{m_j^*}\frac{d\psi_j}{dx}$ at each boundary of the rectangular potential barrier U_j[40], the amplitudes A_j and B_j are correlated with A_{j+1} and B_{j+1} by a 2×2 transfer matrix M_j:

$$\begin{bmatrix} A_j \\ B_j \end{bmatrix} = M_j \begin{bmatrix} A_{j+1} \\ B_{j+1} \end{bmatrix} \tag{4}$$

The transfer matrix M_j in the interval (x_{j-1}, x_j) is given by:

$$M_j = \frac{1}{2}\begin{bmatrix} (1 + S_j)e^{i(k_{j+1}-k_j)x_j} & (1 - S_j)e^{-i(k_{j+1}+k_j)x_j} \\ (1 - S_j)e^{i(k_{j+1}+k_j)x_j} & (1 + S_j)e^{-i(k_{j+1}-k_j)x_j} \end{bmatrix} \tag{5}$$

$$S_j = \frac{m_j^*}{m_{j+1}^*}\frac{k_{j+1}}{k_j} \tag{6}$$

Accordingly, the amplitudes A_0 and B_0 at the left boundary of the arbitrarily shaped potential barrier can be correlated with the amplitudes A_{N+1} and B_{N+1} at the right boundary by the following formula

$$\begin{bmatrix} A_0 \\ B_0 \end{bmatrix} = \prod_{j=0}^{N} M_j \begin{bmatrix} A_{N+1} \\ B_{N+1} \end{bmatrix} = M \begin{bmatrix} A_{N+1} \\ B_{N+1} \end{bmatrix} \tag{7}$$

where

$$M = \begin{bmatrix} M_{11} & M_{12} \\ M_{21} & M_{22} \end{bmatrix} \tag{8}$$

By setting $B_{N+1} = 0$ since there is no reflection at right side of the total potential barrier, the transmission coefficient T of particle tunneling the potential barrier can be expressed as follows:

$$T = \frac{m_0^*}{m_{N+1}^*}\frac{k_{N+1}}{k_0}\left(\frac{A_{N+1}}{A_0}\right)^2 = \left(\frac{1}{M_{11}}\right)^2 \tag{9}$$

which indicates the probability of the particle tunneling through the arbitrarily shaped potential barrier. It should be noted here that, for the carriers in semiconductors, their effective masses will change when tunneling through the interface of the semiconductor heterojunction owing to the different periodic potentials of semiconductors [40]. Though, in our work, the effective masses of carriers in all the regions are taken as those values in Si for convenience. As a result, the difference of the semiconductors' periodic potentials is included in the total potential energy of Si/TiO_2 heterojunction.

3. Results and discussion

The band alignment of the Si/TiO_2 heterojunction and the relative position of the redox potentials for water electrolysis are shown in
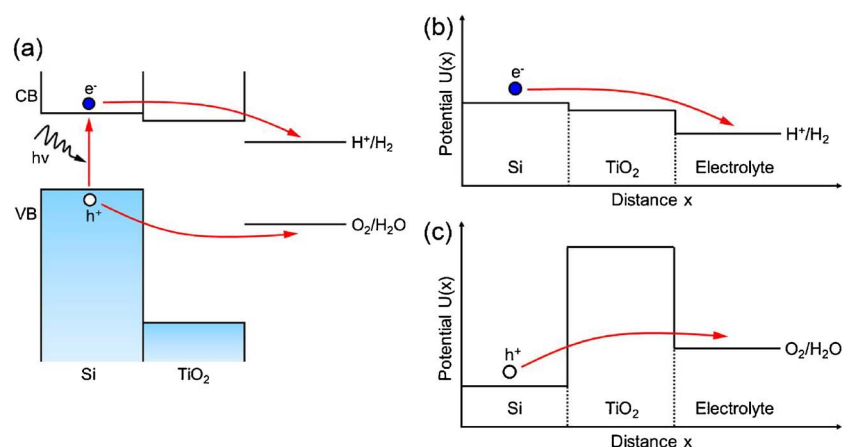
Fig. 2. (a) The schematic energy band diagram of the Si/TiO₂ heterojunction and the redox potentials for solar water splitting; (b) the potential steps for electrons (e⁻) composed by the conduction band (CB) edges of Si and TiO₂ along with the H⁺/H₂ redox potential; (c) the potential barrier for holes (h⁺) composed by the valence band (VB) edges of Si and TiO₂ along with the O₂/H₂O redox potential. The blue and white circles represent electrons and holes, respectively. The red arrows indicate the movements of electron-hole pairs generated by photon (hν) adsorption during photocatalytic water splitting. (For interpretation of the references to colour in this figure legend, the reader is referred to the web version of this article.)

Fig. 2(a). In the process of photocatalytic water splitting, photo-generated electrons (holes) diffusion along the conduction (valence) bands of Si and TiO₂ into the electrolyte. For electrons, the conduction band edges of Si and TiO₂ as well as the H^+/H_2 redox potential form the potential steps (Fig. 2(b)). While for holes, the valence band edges of Si and TiO₂ as well as the O_2/H_2O redox potential form the potential barrier (Fig. 2(c)).

Because the visible light is the strongest output range of the entire solar irradiation spectrum, we mainly focus on the transmission coefficient of charge carrier in visible light range. The photon energy of visible light varies from 1.59 to 3.26 eV according to its wavelength range (380 nm ~ 780 nm). The incident energy of charge carrier in Si is equal to the difference between the adsorbed photon energy and the bandgap energy of Si (1.12 eV), which varies from 0.47 to 2.14 eV. Fig. 3 shows the transmission coefficient $T(E)$ of electrons (holes) in Si tunneling through the potential steps (barrier) as shown in Fig. 2(b) (Fig. 2(c)) with incident energy E. For the electrons in Si, when the thickness of TiO₂ in Si/TiO₂ hetrostructure varies from 0.5 nm to 7 nm, their transmission coefficients $T(E)$ are all larger than 0.95 in the whole range of incident energy E throughout the visible light adsorption (shown in Fig. 3(a)). Especially, the transmission coefficient $T(E)$ is close to one when the incident energy E is larger than 0.9 eV. It indicates that the electron can almost completely tunneling through the Si/TiO₂ heterostructure due to the descending potential steps (Fig. 2(b)). While for the holes in Si, under different TiO₂ thicknesses, their transmission coefficients $T(E)$ are all below 0.4 in the whole range of incident energy E throughout the visible light adsorption and decay rapidly towards the low energy direction (shown in Fig. 3(b)) because the height of the potential barrier (2.23 eV) is larger than the incident energies of holes. Besides, when the TiO₂ thickness is larger 3 nm, the transmission coefficient $T(E)$ of holes is nearly zero, which means that the hole in Si is hard to tunneling into the electrolyte through Si/TiO₂ hetrostructure in this situation. Thus, in these simplified rectangular potential models, only if the TiO₂ layer is thinner than 3 nm can the water oxidation reaction take place in the visible light region.

It is noted that the band bending at the interfaces of Si/TiO₂ heterojunctions take place and has an important impact on the transmission coefficients of electrons and holes tunneling through these heterojunctions. Therefore, in the next step, we study the influence of band bending on the transportation of charge carriers in Si/TiO₂ heterojunction, which depends on several factors such as the TiO₂ layer thickness, the dopant concentrations in Si and TiO₂ components, the photovoltage and so on. The key to design the Si/TiO₂ heterostructure photocatalyst is to find an optimized condition of TiO₂ thickness and dopant concentrations in Si and TiO₂, under which electrons and holes can approach to the water redox potential with relative small incident energies. Firstly, in order to unravel the dependence of TiO₂ thickness and photovoltage on the transmission coefficients of electrons and holes
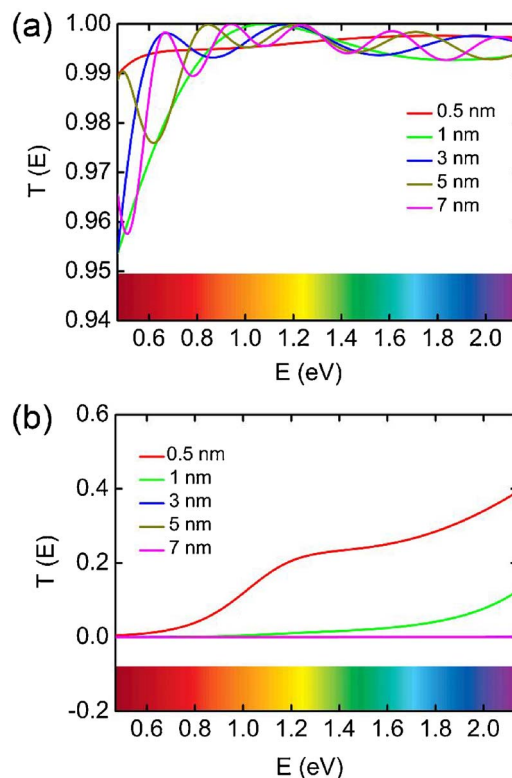
Fig. 3. (a) Transmission coefficient $T(E)$ as a function of incident energy E for electrons tunneling through the potential barrier given in Fig. 2 (b) under different TiO₂ layer thicknesses; (b) Transmission coefficient $T(E)$ as a function of incident energy E for holes tunneling through the potential barrier given in Fig. 2 (c) under different TiO₂ layer thicknesses. The visible adsorption spectrum corresponded with the incident energies of photogenerated carriers are presented at the bottoms of the plots.

tunneling through the Si/TiO₂ heterojunction, the dopant concentrations of Si and TiO₂ are fixed at 1×10^{18} cm⁻³ and 5×10^{19} cm⁻³, respectively.

The total open-circuit phototvoltage V_{ph} of the Si/TiO₂ heterojunction is the sum of open-circuit phototvoltages at Si/TiO₂ and TiO₂/electrolyte interface [44,45]. We denote the voltage produced by the Fermi level difference between Si and electrolyte as V_D. In order to study the effect of photovoltage on carriers' transportation in Si/TiO₂ heterojunction, we calculate the transmission coefficients of electrons and holes without and with photovoltage ($V_{ph} = 0.8$ V).

The depletion width w in semiconductor contacted with electrolyte is calculated as following formula [46,47]:
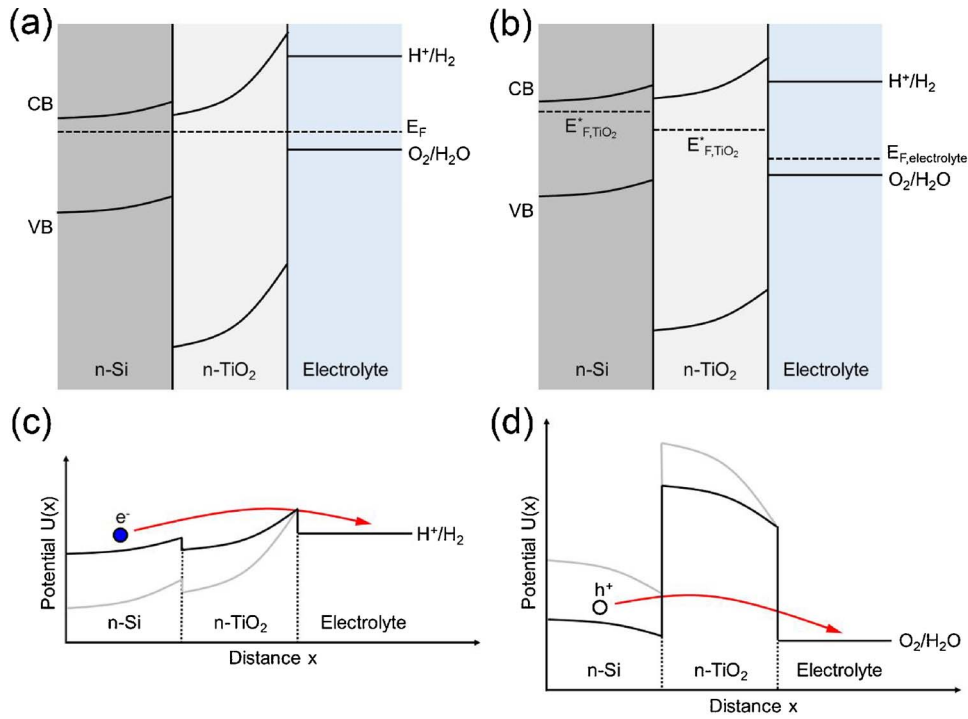
Fig. 4. The energy band diagrams of n-Si/n-TiO$_2$ heterojunctions without photovoltage (a) and with photovoltage (b); (c) the potential barrier for electrons (e$^-$) without photovoltage (gray line) and with photovoltage (black line); (d) the potential barrier for holes (h$^+$) without photovoltage (gray line) and with photovoltage (black line). The blue and white circles represent electrons and holes, respectively. The red arrows indicate the movements of electron-hole pairs generated by photon (hν) adsorption during photocatalytic water splitting. (For interpretation of the references to colour in this figure legend, the reader is referred to the web version of this article.)
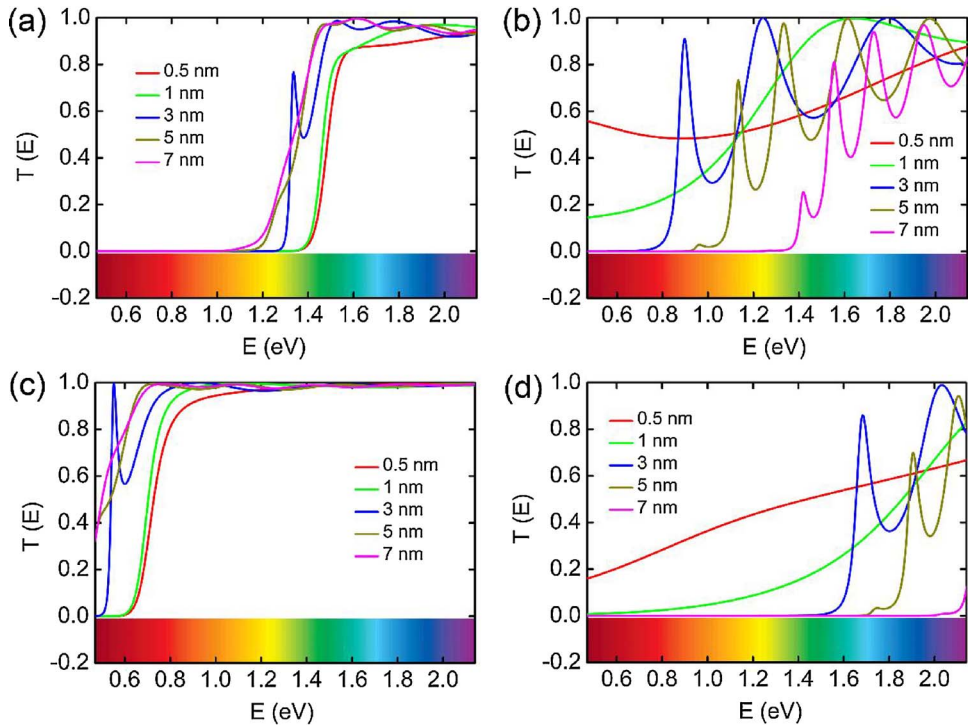

Fig. 5. Transmission coefficient $T(E)$ as a function of incident energy E for electrons tunneling through the potential barrier given in Fig. 4(c) under different TiO$_2$ layer thicknesses without photovoltage (a) and with photovoltage (b); transmission coefficient $T(E)$ as a function of incident energy E for holes tunneling through the potential barriers given in Fig. 4(d) under different TiO$_2$ layer thicknesses without photovoltage (c) and with photovoltage (d). The visible adsorption spectrum corresponded with the incident energies of photogenerated carriers are presented at the bottoms of the plots.

$$w = \left[\frac{2\varepsilon\varepsilon_0(V_{bi} - V_{ph})}{eN_D} \right]^{\frac{1}{2}} \tag{10}$$

where ε is the relative dielectric permittivity of semiconductor, which is set as 32 for TiO$_2$, V_{bi} is the built-in voltage, V_{ph} is the photovoltage under illumination, and N_D is the dopant concentration of semiconductor. When the photovolatage V_{ph} is 0 V and 0.8 V, the depletion width w in TiO$_2$ contacted with electrolyte is estimated to be around 9.7 nm and 7.4 nm, respectively. Since the thickness of the TiO$_2$ protective layer investigated in our work is smaller than those estimated depletion width in TiO$_2$ contacted with electrolyte, the charge carriers

in TiO$_2$ layer will be completely depleted [37]. In consequence, there will be an electric field inside the entire TiO$_2$ layer.

The energy band diagrams for the n-Si/n-TiO$_2$ heterojunction without and with photovoltage ($V_{ph} = 0$ and 0.8 V) are shown in Fig. 4(a) and (b), respectively. When the photovoltage $V_{ph} = 0$ V, the electrons in n-Si and n-TiO$_2$ will transfer into the electrolyte in order to achieving an unified equilibrium Fermi level. Thus, the depletion regions form in both n-Si and n-TiO$_2$. Fig. 5(a) and (b) present the transmission coefficients of electrons and holes in Si tunneling through the potential barriers shown in Fig. 4(c) and (d), respectively. When the thickness of TiO$_2$ layer increases from 0.5 nm to 7 nm, the MIE for
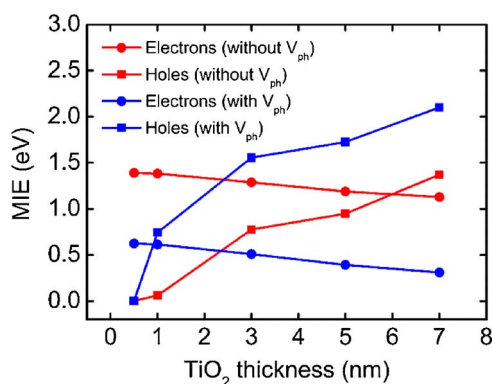
Fig. 6. The MIE for photogenerated electrons and holes tunneling through the Si/TiO$_2$ heterojunction with and without photovoltage V_{ph} as a function of TiO$_2$ layer thickness.

electrons become smaller (Fig. 5(a)). This is attributed to the decreasing effective width and height of potential barriers, which reduces the obstruction for electrons during the transfer process (Fig. 5(c)). The transmission coefficient of electrons in Si is approximate to one when the energy of incident photons is higher than the energy of yellow light. Contrary to the variation trend of potential barriers for electrons, with the increasing TiO$_2$ thickness, the height and width of potential barriers for holes become larger in spite of the total space charge layer width of n-Si/n-TiO$_2$ decreases (Fig. 5(d)). Consequently, holes in Si require more energy to transport across the thicker TiO$_2$ layer (Fig. 5(b)).

The transmission coefficient shown in Fig. 5 is quite different from the results shown in Fig. 3 neglecting the impact of the band bending, which means the band bending at the interface should not be ignored

when analyzing the charge transfer process of heterojunction. For Si/TiO$_2$ photocatalyst, compared with the results neglecting the impact of the band bending, the MIE for electrons (holes) in Si transferring across the same thickness of TiO$_2$ layer shown in Fig. 5 become larger (smaller).

When the n-Si/n-TiO$_2$ heterojunction is under the illumination of UV and visible light, the photogenerated carriers in space charge layer move to different directions under the effect of build-in electric field, which forms an opposite field and weakens the original electric-field strength. When the photovoltage is 0.8 V, the band bending at the semiconductor interface decreases to 0.78 V. As illustrated in Fig. 4(b), the photogenerated holes in Si move toward the n-Si/n-TiO$_2$ interface, while photogenerated electrons in Si are reflected back into the Si layer due to the large potential barrier until they have sufficient energy to be injected into TiO$_2$.

Similar to the results when photovoltage is 0 V (Fig. 5(a) and (b)), as the TiO$_2$ thickness systematically increases from 0.5 nm to 7 nm, the MIE for photogenerated electrons in Si become smaller while that for photogenerated holes in Si become larger (Fig. 5(c) and (d)). Fig. 6 shows the MIE for electrons and holes in Si when the TiO$_2$ thickness changes with and without photovoltage. From Fig. 6, the MIE of holes is much more sensitive to the TiO$_2$ thickness than that of electrons and can be adjusted flexibly by changing the thickness of TiO$_2$ layer. When transferring through the TiO$_2$ layer with the same thickness (0.5 ~ 7 nm), the MIE for photogenerated electrons with photovoltage is ~ 0.8 eV lower than the energy for electrons without photovoltage, while for the photogenerated holes, the MIE with photovoltage is ~ 0.8 eV higher than that without photovoltage. In other words, under the effect of photovoltage, photogenerated electrons can satisfy the potential requirement for water reduction with lower incident energy,
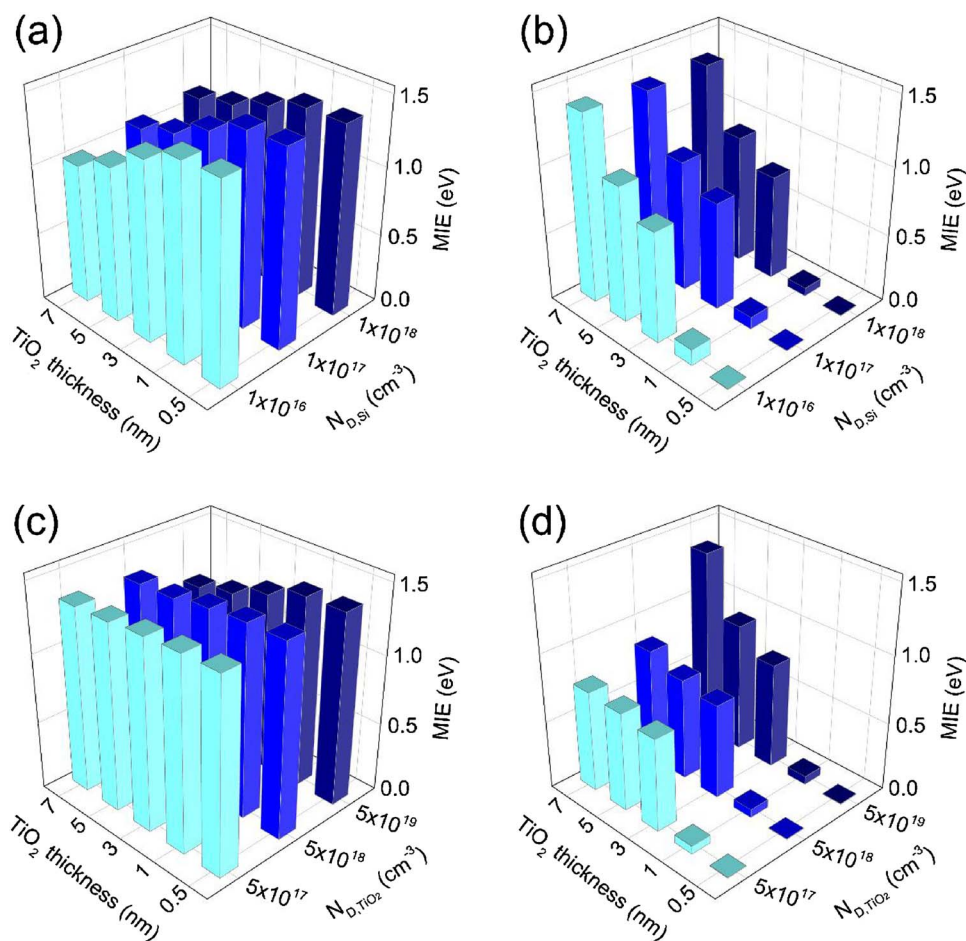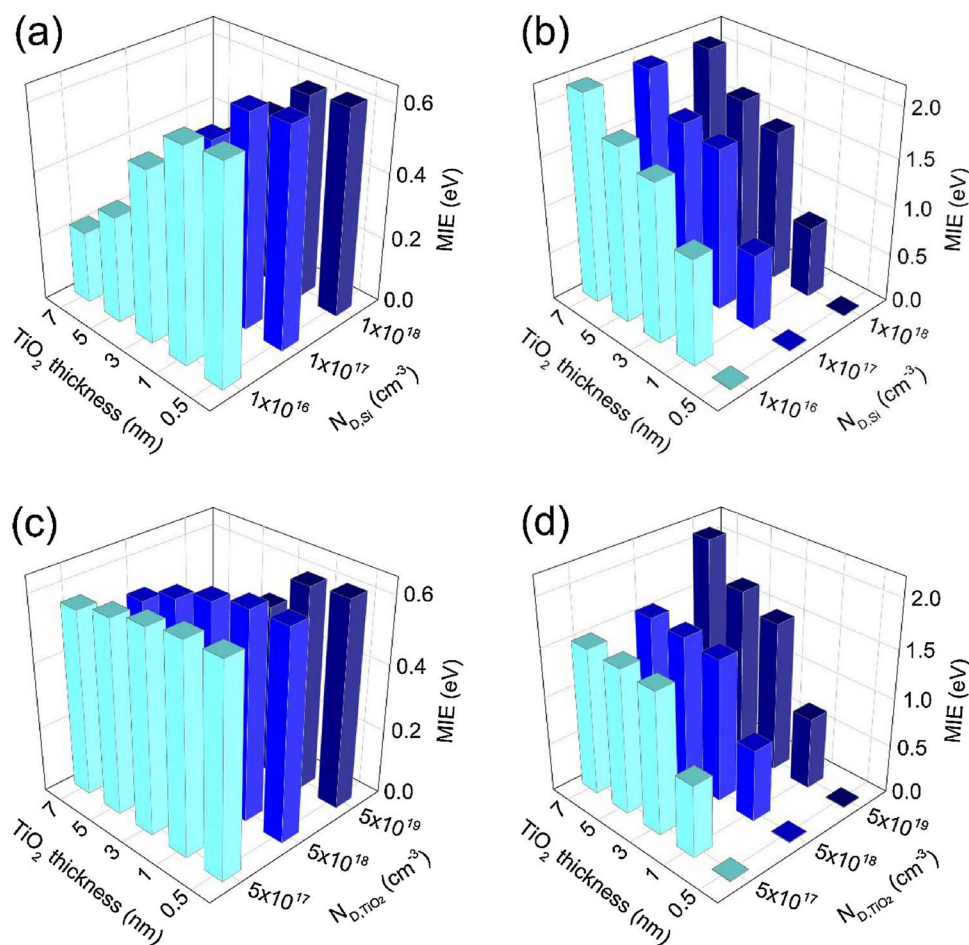

Fig. 7. The MIE for electrons (a) and holes (b) under different dopant concentrations of Si $N_{D,Si}$ and TiO$_2$ thicknesses without photovoltage; the MIE for (c) electrons and (d) holes under different dopant concentrations of TiO$_2$ $N_{D,TiO2}$ and TiO$_2$ thicknesses without photovoltage.

while photogenerated holes in Si need higher incident energy to satisfy the potential requirement for water oxidation. This occurs because the field strength and the band bending within space charge layer are greatly weakened, and the height of potential for photogenerated electrons (holes) in Si increases (decreases) remarkably (Fig. 4(c) and (d)). By choosing a moderate TiO$_2$ thickness, such as 3 nm, the MIE for electrons and holes is relatively low, so the water redox potential can be satisfied with comparatively low incident energy.

The dopant concentration of heterojunction components is another factor that affects the potential distribution in space charge layer. Thereby, we also investigate the influence of Si/TiO$_2$ heterojunction's dopant concentration on the charge transfer process. We firstly fix the dopant concentration of TiO$_2$ at 5×10^{19} cm^{-3} and change the dopant concentration of Si within three different values: 1×10^{16} cm^{-3}, 1×10^{17} cm^{-3} and 1×10^{18} cm^{-3}. As shown in Fig. 7(a) and (b), when the dopant concentration of Si changes, the MIE for electrons and holes transferring across the TiO$_2$ layer with the same thickness is almost invariant. Furthermore, under the same dopant concentration of Si, the MIE for electrons (holes) tunneling across the heterojunction decreases slowly (increases notably) with increasing thickness of TiO$_2$ layer from 0.5 nm to 7 nm. This is due to considerably larger dopant concentration of TiO$_2$ layer than that of Si, thus the potential is mainly distributed in TiO$_2$ layer and nearly unchanged within different dopant concentrations of Si.

Next, we fix the dopant concentration of Si at 1×10^{18} cm^{-3} and change the dopant concentration of TiO$_2$ layer within three values: 5×10^{17} cm^{-3}, 5×10^{18} cm^{-3} and 5×10^{19} cm^{-3}. As shown in Fig. 7(c) and (d), when the TiO$_2$ dopant concentration is 5×10^{17} cm^{-3} or 5×10^{18} cm^{-3}, the MIE for electrons transferring across the heterojunction is nearly invariant with different TiO$_2$

thickness from 0.5 nm ~7 nm, while the MIE for holes firstly increases and then remains almost unchanged with the increasing TiO$_2$ thickness from 0.5 nm ~7 nm. This is because the width of space charge layer in Si is greatly larger than the thickness of TiO$_2$ layer, the potential is mainly distributed in Si and changing the TiO$_2$ thickness has little impact on the potential distribution. However, when the dopant concentration of TiO$_2$ layer (5×10^{19} cm^{-3}) is much larger than that of Si (1×10^{18} cm^{-3}), the potential will mainly distributed in TiO$_2$ layer and vary with different TiO$_2$ thickness, resulting in the notable change of the MIE for electrons and holes as the TiO$_2$ thickness increases.

As shown in Fig. 8, when the photovoltage of Si/TiO$_2$ heterojunction is 0.8 V under illumination, the overall trend of MIE for electrons and holes tunneling through the heterojunction with different dopant concentrations is similar to that without photovoltage (Fig. 7). The difference is that, under the same TiO$_2$ thickness and dopant concentration, the corresponding MIE for photogenerated electrons (holes) becomes smaller (larger), which means that the photogenerated electrons (holes) can transfer across the heterojunction and approach to the water reduction (oxidation) potential with lower (higher) incident energy.

The design and optimization of Si/TiO$_2$ heterojunction photocatalytic system needs to comprehensively considering the influences of dopant concentration and TiO$_2$ thickness. The smaller incident energies electrons and holes need when tunneling through the heterojunction, the more easily they satisfy the water redox potential within visible light range. According to the above discussion, the MIE required by electrons and holes transferring across the heterojunction can be adjusted by varying the thickness of TiO$_2$ layer when the doping concentration of Si and TiO$_2$ are 1×10^{18} cm^{-3} and 5×10^{19} cm^{-3}, respectively. A moderate 3 nm thickness of TiO$_2$ will favor both electrons

and holes satisfy the water redox potential with relatively lower incident energy.

4. Conclusion

In conclusion, the transfer matrix method is adopted to quantitatively analyze the charge transfer process in Si/TiO$_2$ heterojunction photocatalyst. The results show that the band bending and the photovoltage have a significant influence on charge transfer. The degree of band bending is relevant to the thickness of TiO$_2$ layer and the dopant concentrations of heterojunction components. The thicker TiO$_2$ layer is beneficial for electrons approaching to the reduction potential of H$^+$/H$_2$ with relatively lower incident energy, whereas it will lead to the larger MIE for holes transferring to the oxidation potential of O$_2$/H$_2$O. By choosing a moderate condition (TiO$_2$ thickness is 3 nm, dopant concentration of Si and TiO$_2$ are 1×10^{18} cm^{-3} and 5×10^{19} cm^{-3} respectively), both electrons and holes can transfer through the heterojunction barrier with relatively small incident energy. It is noted that the previous experimental reports [10,11] mainly focused on the morphological control of the samples. The intrinsic characteristics of heterojunction (TiO$_2$ thickness and the dopant concentration), which are the essential factor influencing charge transfer in heterojunction, have not been considered in these experimental reports. Considering these intrinsic properties, our work thus provides a valuable design and optimization strategy to further improve the photoactivity of Si/TiO$_2$ heterojunction. Also, our conclusions could be applied to other heterojunction phtotcatalysts, such as Si/ZnO and Si/Fe$_2$O$_3$, with the given dopant concentration and dielectric constant of each side material.

Acknowledgments

Appendix A. Supplementary data

Supplementary data associated with this article can be found, in the online version, at http://dx.doi.org/10.1016/j.apcatb.2017.08.087.

References

[1] N.S. Lewis, D.G. Nocera, Powering the planet: chemical challenges in solar energy utilization, Proc. Natl. Acad. Sci. 103 (2006) 15729–15735.
[2] O. Khaselev, J.A. Turner, A monolithic photovoltaic-photoelectrochemical device for hydrogen production via water splitting, Science 280 (1998) 425–427.
[3] M. Gratzel, Photoelectrochemical cells, Nature 414 (2001) 338–344.
[4] J. Nowotny, C.C. Sorrell, L.R. Sheppard, T. Bak, Solar-hydrogen: environmentally safe fuel for the future, Int. J. Hydrogen Energy 30 (2005) 521–544.
[5] P. Lianos, Review of recent trends in photoelectrocatalytic conversion of solar energy to electricity and hydrogen, Appl. Catal. B: Environ. 210 (2017) 235–254.
[6] A. Fujishima, K. Honda, Electrochemical photolysis of water at a semiconductor electrode, Nature 238 (1972) 37–38.
[7] M.G. Walter, E.L. Warren, J.R. McKone, S.W. Boettcher, Q. Mi, E.A. Santori, N.S. Lewis, Solar water splitting cells, Chem. Rev. 110 (2010) 6446–6473.
[8] Z. Zou, J. Ye, K. Sayama, H. Arakawa, Direct splitting of water under visible light irradiation with an oxide semiconductor photocatalyst, Nature 414 (2001) 625–627.
[9] X. Chen, S. Shen, L. Guo, S.S. Mao, Semiconductor-based photocatalytic hydrogen generation, Chem. Rev. 110 (2010) 6503–6570.
[10] H. Yu, S. Chen, X. Quan, H. Zhao, Y. Zhang, Silicon nanowire/TiO$_2$ heterojunction arrays for effective photoelectrocatalysis under simulated solar light irradiation, Appl. Catal. B: Environ. 90 (2009) 242–248.
[11] Y.J. Hwang, A. Boukai, P. Yang, High density n-Si/n-TiO$_2$ core/shell nanowire arrays with enhanced photoactivity, Nano Lett. 9 (2009) 410–415.
[12] H. Zhu, B. Yang, J. Xu, Z. Fu, M. Wen, T. Guo, S. Fu, J. Zuo, S. Zhang, Construction of Z-scheme type CdS-Au-TiO$_2$ hollow nanorod arrays with enhanced photocatalytic activity, Appl. Catal. B: Environ. 90 (2009) 463–469.
[13] H. Tada, T. Mitsui, T. Kiyonaga, T. Akita, K. Tanaka, All-solid-state Z-scheme in CdS-Au-TiO$_2$ three-component nanojunction system, Nat. Mater. 5 (2006) 782–786.
[14] A. Iwase, Y.H. Ng, Y. Ishiguro, A. Kudo, R. Amal, Reduced graphene oxide as a solid-state electron mediator in Z-scheme photocatalytic water splitting under visible light, J. Am. Chem. Soc. 133 (2011) 11054–11057.
[15] P. Zhou, J. Yu, M. Jaroniec, All-solid-state z-scheme photocatalytic systems, Adv. Mater.

[16] 26 (2014) 4920–4935.
L. Ye, J. Liu, C. Gong, L. Tian, T. Peng, L. Zan, Two different roles of metallic ag on Ag/AgX/BiOX (X = Cl, Br) visible light photocatalysts: surface plasmon resonance and Z-scheme bridge, ACS Catal. 2 (2012) 1677–1683.
[17] Y. Wang, Q. Wang, X. Zhan, F. Wang, M. Safdar, J. He, Visible light driven type II heterostructures and their enhanced photocatalysis properties: a review, Nanoscale 5 (2013) 8326–8339.
[18] Y. Tak, H. Kim, D. Lee, K. Yong, Type-II CdS nanoparticle-ZnO nanowire heterostructure arrays fabricated by a solution process: enhanced photocatalytic activity, Chem. Commun. (2008) 4585–4587.
[19] D. Sarkar, C.K. Ghosh, S. Mukherjee, K.K. Chattopadhyay, Three dimensional Ag$_2$O/TiO$_2$ type-II (p-n) nanoheterojunctions for superior photocatalytic activity, ACS Appl. Mater. Interfaces 5 (2013) 331–337.
[20] M. Basu, N. Garg, A.K. Ganguli, A type-II semiconductor (ZnO/CuS heterostructure) for visible light photocatalysis, J. Mater. Chem. A 2 (2014) 7517–7525.
[21] Z. Zhang, J.T. Yates, Band bending in semiconductors: chemical and physical consequences at surfaces and interfaces, Chem. Rev. 112 (2012) 5520–5551.
[22] M.J. Kenney, M. Gong, Y. Li, J.Z. Wu, J. Feng, M. Lanza, H. Dai, High-performance silicon photoanodes passivated with ultrathin nickel films for water oxidation, Science 342 (2013) 836–840.
[23] Y.J. Hwang, C.H. Wu, C. Hahn, H.E. Jeong, P. Yang, Si/InGaN core/shell hierarchical nanowire arrays and their photoelectrochemical properties, Nano Lett. 12 (2012) 1678–1682.
[24] R.N. Dominey, N.S. Lewis, J.A. Bruce, D.C. Bookbinder, M.S. Wrighton, Improvement of photoelectrochemical hydrogen generation by surface modification of p-type silicon semiconductor photocathodes, J. Am. Chem. Soc. 104 (1982) 467–482.
[25] S. Li, P. Zhang, X. Song, L. Gao, Photoelectrochemical hydrogen production of TiO$_2$ passivated Pt/Si-nanowire composite photocathode, ACS Appl. Mater. Interfaces 7 (2015) 18560–18565.
[26] A. Kargar, K. Sun, Y. Jing, C. Choi, H. Jeong, Y. Zhou, K. Madsen, P. Naughton, S. Jin, G.Y. Jung, D. Wang, Tailoring n-ZnO/p-Si branched nanowire heterostructures for selective photoelectrochemical water oxidation or reduction, Nano Lett. 13 (2013) 3017–3022.
[27] B. Seger, T. Pedersen, A.B. Laursen, P.C.K. Vesborg, O. Hansen, I. Chorkendorff, Using TiO$_2$ as a conductive protective layer for photocathodic H$_2$ evolution, J. Am. Chem. Soc. 135 (2013) 1057–1064.
[28] S. Hu, M.R. Shaner, J.A. Beardslee, M. Lichterman, B.S. Brunschwig, N.S. Lewis, Amorphous TiO$_2$ coatings stabilize Si, GaAs, and GaP photoanodes for efficient water oxidation, Science 344 (2014) 1005–1009.
[29] K. Rajeshwar, Hydrogen generation at irradiated oxide semiconductor-solution interfaces, J. Appl. Electrochem. 37 (2007) 765–787.
[30] K. Kitano, M. Matsuoka, M. Ueshima, M. Anpo, Recent developments in titanium oxide-based photocatalysts, Appl. Catal. A: Gen. 325 (2007) 1–14.
[31] M. Pelaez, N.T. Nolan, S.C. Pillai, M.K. Seery, P. Falaras, A.G. Kontos, P.S.M. Dunlop, J.W.J. Hamilton, J.A. Byrne, K. O'Shea, M.H. Entezari, D.D. Dionysiou, A review on the visible light active titanium dioxide photocatalysts for environmental applications, Appl. Catal. B: Environ. 125 (2012) 331–349.
[32] M.T. Mayer, C. Du, D. Wang, Hematite/Si nanowire dual-absorber system for photoelectrochemical water splitting at low applied potentials, J. Am. Chem. Soc. 134 (2012) 12406–12409.
[33] S. Takabayashi, R. Nakamura, Y. Nakato, A nano-modified Si/TiO$_2$ composite electrode for efficient solar water splitting, J. Photochem. Photobiol. A: Chem. 166 (2004) 107–113.
[34] H. Morisaki, T. Watanabe, M. Iwase, K. Yazawa, Photoelectrolysis of water with TiO$_2$-covered solar-cell electrodes, Appl. Phys. Lett. 29 (1976) 338–340.
[35] C.Y. Lin, Y.K. Fang, C.H. Kuo, S.F. Chen, C.-S. Lin, T.H. Chou, Y.-H. Lee, J.-C. Lin, S.-B. Hwang, Design and fabrication of a TiO$_2$/nano-silicon composite visible light photocatalyst, Appl. Surf. Sci. 253 (2006) 898–903.
[36] X. Zhang, Y. Wang, B. Liu, Y. Sang, H. Liu, Heterostructures construction on TiO$_2$ nanobelts: a powerful tool for building high-performance photocatalysts, Appl. Catal. B: Environ. 202 (2017) 620–641.
[37] X. Qi, G. She, X. Huang, T. Zhang, H. Wang, L. Mu, W. Shi, High-performance n-Si/α-Fe$_2$O$_3$ core/shell nanowire array photoanode towards photoelectrochemical water splitting, Nanoscale 6 (2014) 3182–3189.
[38] D. Perera, R. Lorek, R.S. Khnayzer, P. Moroz, T. O'Connor, D. Khon, G. Diederich, E. Kinder, S. Lambright, F.N. Castellano, M. Zamkov, Photocatalytic activity of core/shell semiconductor nanocrystals featuring spatial separation of charges, J. Phys. Chem. C 116 (2012) 22786–22793.
[39] X. Li, J. Chen, H. Li, J. Li, Y. Xu, Y. Liu, J. Zhou, Photoreduction of CO$_2$ to methanol over Bi$_2$S$_3$/CdS photocatalyst under visible light irradiation, J. Nat. Gas Chem. 20 (2011) 413–417.
[40] A.F.J. Levi, Applied Quantum Mechanics, Cambridge University Press, 2006.
[41] Z. Hui-yun, G. Ying, Z. Yu-ping, X. Shi-lin, W. Shi-fan, A tunable electron wave filter based on graphene superlattices with periodic potential patterns, Appl. Phys. Lett. 99 (2011) 072108.
[42] A.K. Ghatak, K. Thyagarajan, M.R. Shenoy, A novel numerical technique for solving the one-dimensional Schroedinger equation using matrix approach-application to quantum well structures, IEEE J. Quantum Electron. 24 (1988) 1524–1531.
[43] H. Cruz, Resonant tunneling through parabolic quantum wells achieved by means of short period superlattices, Solid State Commun. 85 (1993) 65–68.
[44] S. Wagner, J.L. Shay, n-CdS/n-GaAs voltage-enhanced photoanode, Appl. Phys. Lett. 31 (1977) 446–447.
[45] M.F. Weber, M.J. Dignam, Efficiency of splitting water with semiconducting photoelectrodes, J. Electrochem. Soc. 131 (1984) 1258–1265.
[46] X. Yang, A. Wolcott, G. Wang, A. Sobo, R.C. Fitzmorris, F. Qian, J.Z. Zhang, Y. Li, Nitrogen-doped ZnO nanowire arrays for photoelectrochemical water splitting, Nano Lett. 9 (2009) 2331–2336.
[47] M.X. Tan, P.E. Laibinis, S.T. Nguyen, J.M. Kesselman, C.E. Stanton, N.S. Lewis, Principles and applications of semiconductor photoelectrochemistry, Progress in Inorganic Chemistry, John Wiley & Sons, Inc., 2007, pp. pp. 21–144.